https://doi.org/10.1016/j.jsv.2018.12.037

Vibration Characteristics Analysis of Magnetically Suspended Rotor in Flywheel Energy Storage System

Biao Xiang and Wai on Wong
Department of Mechanical Engineering,
The Hong Kong Polytechnic University, Kowloon, HKSAR, China

ABSTACT

A clear understanding of the vibration characteristics of the magnetically suspended rotor (MSR) in the flywheel energy storage system is critical to its stability and control precision. Therefore, the detailed relationship between the vibration characteristics of the MSR and system parameters is modeled and analyzed experimentally in this article. The stiffness of the MSR is tunable by regulating the proportional coefficient of the control system such that the desirable natural frequency of the MSR can be achieved. Moreover, the vibration transmissibility of the MSR is controllable by regulating damping parameters of control system. Therefore, this analysis and experimental results are useful for the design and control of the whole system. In addition, the tilting vibration characteristics of the MSR with different disturbance torques are analyzed. The tilting response angle of MSR is affected by natural frequency of rotor and the frequency of the disturbance input. The results present the relationship between the vibration dynamics of the MSR and the disturbance torques, which is meaningful for the control of the MSR with disturbance torques.

Keyword: magnetically suspended rotor; vibration transmissibility; vibration characteristics; disturbance torque.

1. Introduction

The magnetic suspension technology is widely used in rotational machineries such as energy storage and attitude control flywheel [1, 2], control moment gyro for satellite [3-6], high energy density motor [7, 8], molecular pump [9-14] and inertial stabilized platform [15-17] because of its zero-friction, lubrication free, longevity and active controllability. For the MSR system, there is no contact between the rotor and the stator, so the vibration disturbances can be effectively isolated, and the loss caused by the friction between the rotor and the stator in the mechanical suspension system such as mechanical bearing and gear can be eliminated [18-20]. Moreover, when the rotor runs at a high-speed, the active controllability of magnetic suspension system can keep the rotor run stably by regulating the control current based on the displacement feedback and vibration signal of rotor [21-24]. Therefore, comparing with ordinary rotational machineries with mechanical bearings and gears, the MSR has the advantages of high stability margin, low power consumption and longevity.

A clear understanding of vibration characteristics of the MSR is critical to stability and control precision. Asama et al. [25] proposed a five-axis actively controllable bearingless permanent magnet motor with non-contact magnetic suspension system which offer advantages of no wear particles, less maintenance, and high rotational speed as compared to mechanical suspension system that causes mechanical friction. Tang et al. [26] investigated the dynamic characteristics of the MSR in the magnetically suspended control moment gyro with active magnetic bearing (AMB) and passive magnetic bearing, and its modal shapes was affect by the current stiffness. Ji and Hansen [27] studied nonlinear characteristics of the MSR at resonances and the effect of the proportional and derivative control gains on the nonlinear response characteristics by numerical simulation. Ji et al. [28] analyzed the nonlinear dynamics of a rigid rotor suspended by AMB. They discovered that the vibration characteristics in radial and axial directions were affected by the rotor mass. Yan et al. [29] analyzed the stator vibration of bearingless switched reluctance motor with magnetic suspension system. They found that the stator vibration of bearingless switched reluctance motor is smaller and radiate less noise than the ordinary switched reluctance motor. Yang [30] discovered that radial oscillations of miniature magnetically levitated rotating machine became excessively large when the rotational frequency was close to the resonate frequency. He proposed a control scheme for the electromagnetic actuator to suppress the resonance-related oscillation of rotor. Tang et al. [31] analyzed mechanical characteristics of the high-speed rotor in a magnetically suspended control moment gyro. Results of their analysis indicated that the control stability of the high-speed MSR highly depends on the moment of inertia ratio which is decided by the rotor mass and material density, and generalized stiffness and shape coefficient.

There are many research reports on vibration characteristics of MSR in literature, but the relationship between vibration characteristics and system parameters of MSR is still not clear. In this article, vibration characteristics of a MSR in a flywheel energy storage system is modeled and tested experimentally. The relationships amongst the vibration, system parameters and control coefficients are derived and tested experimentally. The analysis and experimental results are useful for the design and realization of the control system for the MSR.

2. Work Principle of MSR

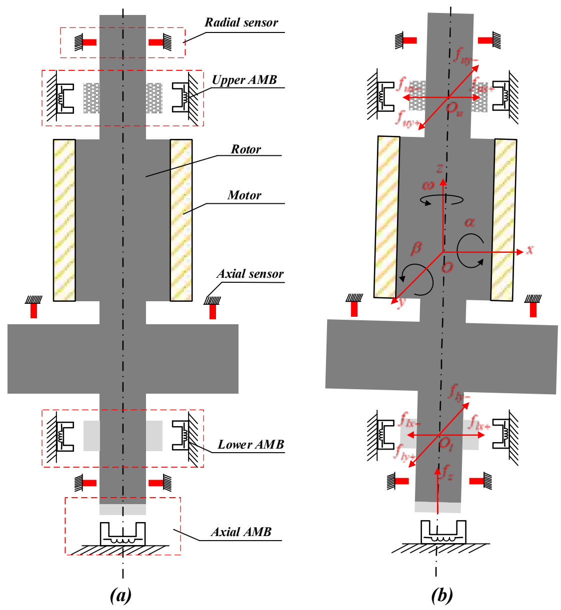

Fig. 1. Structure of MSR, (a) structure, (b) forces analysis of rotor.

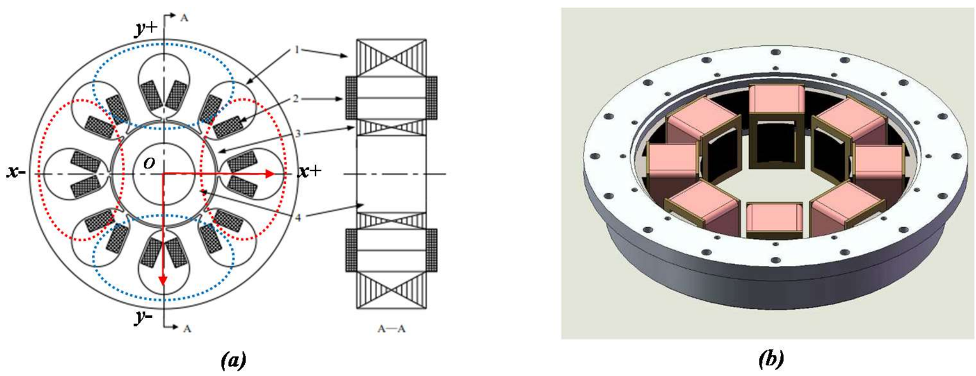

Fig. 2. Radial AMB, (a) cross-sectional view, (b) stator part of AMB.

As illustrated in Fig. 1(a), the MSR system is suspended by the radial and axial suspension system. The radial suspension system contains two pairs of AMBs. The pair of lower AMBs generate suspension force (f_{lx+} and f_{lx-}, f_{ly+} and f_{ly-}) to control the lower radial motion of rotor while the pair of upper AMBs generate suspension force (f_{ux+} and f_{ux-}, f_{uy+} and f_{uy-}) to control the upper radial motion of rotor. Consequently, the tilting around x axis and y axis is controlled by the resultant suspension forces of lower AMBs and upper AMBs. On the other hand, the axial suspension force f_z generated by axial AMB makes rotor stably suspended at the axial equilibrium point.

The structure of radial AMB is shown in Fig. 2. It consists of eight independent AMBs, and so the magnetic suspension system can realize the decentralized and differential control of rotor in each direction. The magnetic suspension force generated by the AMB can be expressed as

$$f(i,d)=\frac{\mu_0 AN^2}{4}\cdot\frac{i^2}{d^2} \tag{1}$$

where μ_0 is the vacuum permeability. A is the cross-sectional area. N is the number of turn. i is the current of winding, and d is the air-gap between the rotor and the stator. Differential control of the MSR is applied and the resultant magnetic suspension force in x axis can be written as

$$\begin{aligned} f_x(i_x,d_x)=f_{x+}-f_{x-}&=\frac{\mu_0 AN^2}{4}\left[\frac{(i_0+i_x)^2}{(d_0-d_x)^2}-\frac{(i_0-i_x)^2}{(d_0+d_x)^2}\right] \\ &=\frac{\mu_0 AN^2}{4}\cdot\frac{i_0 i_x d_0^2+i_x^2 d_0 d_x+i_0^2 d_0 d_x+i_0 i_x d_x^2}{(d_0-d_x)^2(d_0+d_x)^2} \\ &=\frac{\mu_0 AN^2}{4}\cdot\frac{i_0 i_x d_0^2+i_x^2 d_0 d_x+i_0^2 d_0 d_x+i_0 i_x d_x^2}{d_0^4-2d_0^2 d_x^2+d_x^4} \end{aligned} \tag{2}$$

Since the rotor displacement d_x in x axis is relatively small when comparing with the bias air-gap between the rotor and the stator d_0, Eq. (2) may be approximately written as

$$f_x(i_x,d_x)=\frac{\mu_0 AN^2 i_0}{d_0^2}\cdot i_x+\frac{\mu_0 AN^2 i_0^2}{d_0^3}\cdot d_x=k_i\cdot i_x+k_d\cdot d_x \tag{3}$$

where i_0 is the bias current of winding, and i_x is the control current of winding. Eq. (3) shows that the magnetic suspension force f_x is proportional to the control current i_x and rotor displacement d_x. Since the bias current i_0 and the bias air-gap d_0 are constant, the current stiffness and the displacement stiffness can be respectively written as

$$k_i=\frac{\mu_0 AN^2 i_0}{d_0^2} \tag{4}$$

$$k_d=\frac{\mu_0 AN^2 i_0^2}{d_0^3} \tag{5}$$

The relationship between the magnetic suspension force and control current is shown in Fig. 3(a), which indicates that the magnetic suspension force is proportional to the control current in radial direction, and the current stiffness k_i within the vicinity of the equilibrium point is about 620 *N*/*A*. Fig. 3(b) presents that the magnetic suspension force versus the displacement within the vicinity of the radial equilibrium point. The displacement stiffness k_d is about -2800 N/mm.

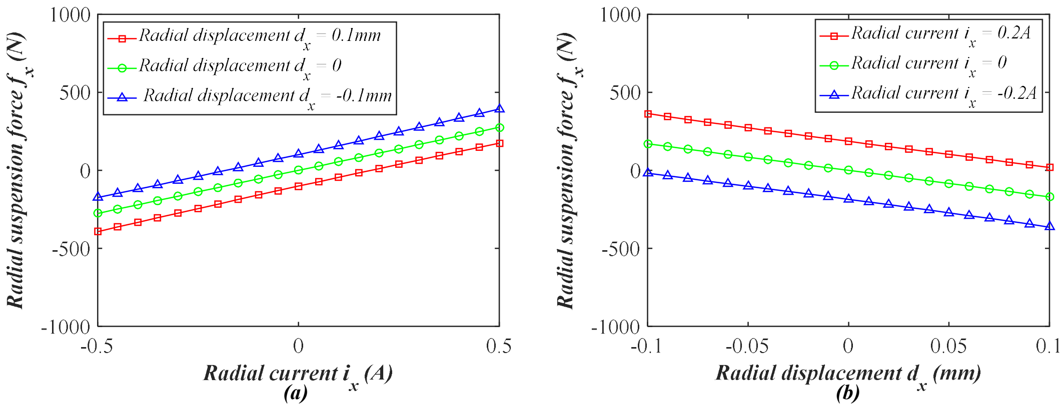

Fig. 3. Radial magnetic suspension force, (a) magnetic suspension force vs. control current, (b) magnetic suspension force vs. displacement.

3. Dynamics Modeling of MSR

3.1. Dynamic Characteristics of MSR

Based on the force analysis in Fig. 1(b), the equation of translational motion of rotor can be written as

$$\begin{cases} m\ddot{d}_x = f_{x+} - f_{x-} \\ m\ddot{d}_y = f_{y+} - f_{y-} \\ m\ddot{d}_z = f_z \end{cases} \tag{6}$$

The equation of rotational motion of rotor can be written as

$$\begin{cases} J_y\ddot{\beta} - J_z\omega\dot{\alpha} = T_x \\ J_x\ddot{\alpha} + J_z\omega\dot{\beta} = T_y \end{cases} \tag{7}$$

where f_{x+} and f_{x-} are magnetic suspension forces in positive and negative directions along x axis, respectively. f_{y+} and f_{y-} are magnetic suspension forces in positive and negative directions along y axis, respectively. J_x and J_y are equatorial moment of inertias of rotor around x axis and y axis, respectively. J_z is the polar moment of inertia of rotor. α and β are the respective tilting angles around x axis and y axis, and ω is the rotational frequency of the MSR.

The relationship between control current and displacement of MSR can be expressed as

$$i_x = k_P d_x + k_D \dot{d}_x \tag{8}$$

where k_P is the proportional coefficient, and k_D is the derivative coefficient. Therefore, the equation of translational motion can be written as

$$m\ddot{d}_x - k_i k_D \dot{d}_x - (k_i k_P + k_d) d_x = f_{dx} \tag{9}$$

Then the natural frequency of translational motion can be expressed as

$$\omega_n = \sqrt{\frac{-(k_i k_P + k_d)}{m}} \tag{10}$$

The damping coefficient is

$$\xi = \frac{-k_D k_i}{2\sqrt{-m(k_i k_P + k_d)}} \tag{11}$$

Therefore, the vibration transmissibility of translational motion can be written as

$$TR = \sqrt{\frac{1 + (2\xi r)^2}{(1 - r^2)^2 + (2\xi r)^2}} \tag{12}$$

where $r = \dfrac{\omega_t}{\omega_n}$ is the frequency ratio, and ω_t is the vibration frequency of translation.

3.2. Rotational Dynamics of MSR

Using rotation functions in Eq. (7), the tilting angle of MSR can be written as

$$J_d \ddot{\varphi} - H\dot{\varphi} i + k_\varphi \varphi = 0 \tag{13}$$

where $\varphi(t) = \alpha(t) + \beta(t) i$, and the characteristic equation can be written as

$$-\omega_{n\varphi}^2 + \frac{J_x}{J_z}\omega\omega_{n\varphi} + \omega_\varphi^2 = 0 \tag{14}$$

where $\omega_\varphi^2 = \dfrac{k_\varphi}{J_z}$, and $\omega_{n\varphi}$ is the whirling angular frequency of MSR. The tilting angular frequencies of forward whirling and backward whirling can be derived and written respectively as

$$\begin{aligned} \omega_f &= \frac{1}{2}\left[\frac{J_x}{J_z}\omega + \sqrt{\left(\frac{J_x}{J_z}\omega\right)^2 + 4\omega_\varphi^2}\right] \\ \omega_b &= \frac{1}{2}\left[\frac{J_x}{J_z}\omega - \sqrt{\left(\frac{J_x}{J_z}\omega\right)^2 + 4\omega_\varphi^2}\right] \end{aligned} \tag{15}$$

It shows that the frequency of the forward whirling ω_f increases with rotational frequency ω, but the frequency of the backward whirling ω_b decreases with rotational frequency ω.

3.3. Dynamic Characteristics of MSR with Disturbances

Given the state vector $\mathbf{x} = [\alpha \quad \dot{\alpha} \quad \beta \quad \dot{\beta}]^T$, input vector $\mathbf{u} = [T_x \quad T_y]^T$, and the output vector $\mathbf{y} = [\alpha \quad \beta]^T$. The state space model of rotational motion can written as

$$\begin{cases} \dot{\mathbf{x}} = \mathbf{A}\mathbf{x} + \mathbf{B}\mathbf{u} \\ \mathbf{y} = \mathbf{C}\mathbf{x} \end{cases} \tag{16}$$

where $\mathbf{A} = \begin{bmatrix} 0 & 1 & 0 & 0 \\ 0 & 0 & 0 & J_z\omega/J_y \\ 0 & 0 & 0 & 1 \\ 0 & -J_z\omega/J_x & 0 & 0 \end{bmatrix}$, $\mathbf{B} = \begin{bmatrix} 0 & 0 \\ 1/J_y & 0 \\ 0 & 0 \\ 0 & 1/J_x \end{bmatrix}$, $\mathbf{C} = \begin{bmatrix} 1 & 0 & 0 & 0 \\ 0 & 0 & 1 & 0 \end{bmatrix}$. The state transformation matrix can be achieved as in the following

$$e^{\mathbf{A}t} = L^{-1}(s\mathbf{I} - \mathbf{A})^{-1} \tag{17}$$

where L^{-1} is the inverse Laplace transformation operator, and $\mathbf{I}$ is the unit matrix.

Given moment of rotation $H = J_z\omega$ and the natural rotational frequency $\omega_{rn} = \dfrac{H}{\sqrt{J_x J_y}}$, the transformation matrix can be obtained as follows.

$$e^{\mathbf{A}t} = \begin{bmatrix} 1 & \dfrac{\sin\omega_{rn}t}{\omega_{rn}} & 0 & \dfrac{J_x(1-\cos\omega_{rn}t)}{H} \\ 0 & \cos\omega_{rn}t & 0 & \dfrac{H\sin\omega_{rn}t}{J_y\omega_{rn}} \\ 0 & \dfrac{-J_y(1-\cos\omega_{rn}t)}{H} & 1 & \dfrac{\sin\omega_{rn}t}{\omega_{rn}} \\ 0 & \dfrac{-H\sin\omega_{rn}t}{J_x\omega_{rn}} & 0 & \cos\omega_{rn}t \end{bmatrix} \tag{18}$$

The solution of state space equation can be written as

$$x(t) = e^{\mathbf{A}t}x(0) + \int_0^t e^{\mathbf{A}(t-\tau)}\mathbf{B}u(\tau)d\tau \tag{19}$$

Assuming the initial condition, $x(0) = 0$, when three typical disturbance torques including transient impact torque, constant torque and harmonic torque are considered to apply separately onto the MSR, the tilting angle response of MSR can be calculated by solving Eq. (19). Considering the input of a transient impulse torque $u(t) = \delta(t)[1 \quad 1]^T$, where $\delta(t)$ is the Dirac delta function. The solution of the state space equation is

$$x(t)=\int_0^t e^{\mathbf{A}(t-\tau)}\mathbf{B}\delta(\tau)[1 \quad 1]^T\,d\tau \tag{20}$$

The tilting angles of MSR can be solved and written as

$$\begin{cases}\alpha(t)=\dfrac{1}{H}\sqrt{\dfrac{J_x}{J_y}}\sin\omega_{rn}t-\dfrac{1}{H}\cos\omega_{rn}t+\dfrac{1}{H}\\ \beta(t)=\dfrac{1}{H}\sqrt{\dfrac{J_x}{J_y}}\sin\omega_{rn}t+\dfrac{1}{H}\cos\omega_{rn}t-\dfrac{1}{H}\end{cases} \tag{21}$$

So the tilting angles α and β of MSR vary with the natural rotational frequency ω_{rn}.

In case of a constant torque input, $u(t)=[1 \quad 1]^T$, solution of the state space equation is

$$x(t)=\int_0^t e^{\mathbf{A}(t-\tau)}\mathbf{B}[1 \quad 1]^T\,d\tau \tag{22}$$

The tilting angles of the MSR can be solved and written as

$$\begin{cases}\alpha(t)=\dfrac{J_x}{H^2}+\dfrac{1}{H}t-\dfrac{\sqrt{J_xJ_y}}{H^2}\sin\omega_{rn}t-\dfrac{J_x}{H^2}\cos\omega_{rn}t\\ \beta(t)=\dfrac{J_y}{H^2}+\dfrac{1}{H}t-\dfrac{\sqrt{J_xJ_y}}{H^2}\sin\omega_{rn}t-\dfrac{J_y}{H^2}\cos\omega_{rn}t\end{cases} \tag{23}$$

It shows that the tilting angles of the MSR also vary with the natural rotational frequency.

For the case of a harmonic torque input, $u(t)=[M_{x0}\sin\omega_x t \quad M_{y0}\sin\omega_y t]^T$, the solution of state space equation can be expressed as

$$x(t)=\int_0^t e^{\mathbf{A}(t-\tau)}\mathbf{B}[M_{x0}\sin\omega_x t \quad M_{y0}\sin\omega_y t]^T\,d\tau \tag{24}$$

The tilting angles of the MSR can be solved and written as

$$\begin{cases}\alpha(t)=\dfrac{M_{x0}}{H\omega_x}-\dfrac{\omega_{rn}^2M_{x0}}{H\omega_x(\omega_{rn}^2-\omega_x^2)}\cos\omega_x t+\dfrac{M_{y0}}{J_y(\omega_{rn}^2-\omega_y^2)}\cos\omega_y t\\ \qquad +\dfrac{\omega_xM_{x0}}{H(\omega_{rn}^2-\omega_x^2)}\cos\omega_{rn}t+\dfrac{\omega_yM_{y0}}{J_y\omega_{rn}(\omega_{rn}^2-\omega_y^2)}\sin\omega_{rn}t\\ \beta(t)=\dfrac{M_{y0}}{H\omega_y}-\dfrac{\omega_{rn}^2M_{y0}}{H\omega_y(\omega_{rn}^2-\omega_y^2)}\cos\omega_y t+\dfrac{M_{x0}}{J_x(\omega_{rn}^2-\omega_x^2)}\cos\omega_x t\\ \qquad -\dfrac{\omega_yM_{y0}}{H(\omega_{rn}^2-\omega_y^2)}\cos\omega_{rn}t-\dfrac{\omega_xM_{x0}}{J_x\omega_{rn}(\omega_{rn}^2-\omega_x^2)}\sin\omega_{rn}t\end{cases} \tag{25}$$

This equation indicates that the tilting angles α and β of MSR varies with the natural rotational frequency ω_{rn} and the frequencies of harmonic input torque ω_x and ω_y.

4. Experiment

4.1. Control Scheme of MSR

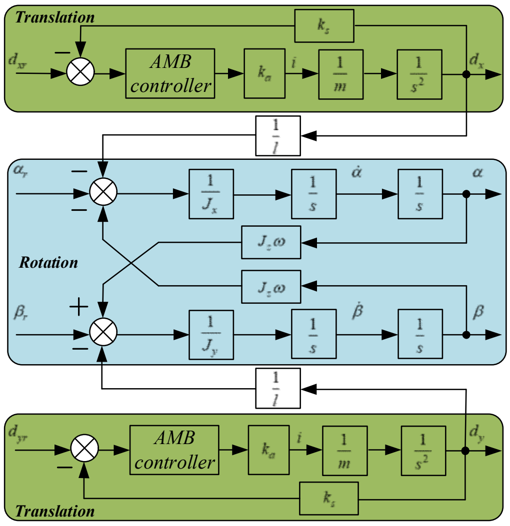

Fig. 4. Control scheme of the MSR.

The whole control scheme of the MSR system is illustrated in Fig. 4, and it contains translational control loop and rotational control loop. The reference displacement $(d_{xr} \quad d_{yr})^T$ and reference angle $(\alpha_r \quad \beta_r)^T$ of the MSR are defined as the system input, and the output of MSR system are $(d_x \quad d_y)^T$ and $(\alpha \quad \beta)^T$. In the control loop of translational motion, the displacement output $(d_x \quad d_y)^T$ measured by eddy current displacement sensors are used as feedback signals. Based on these feedback signals, the controller generates control current to realize the differential control of the MSR. In the control loop of rotational motion, the tilting angle based on the displacement feedback is chosen as the input. In addition, the cross compensation with speed feedback is applied to suppress the gyroscopic effect of MSR, and then the nutation vibration of the MSR is mitigated.

4.2. Experimental Setups

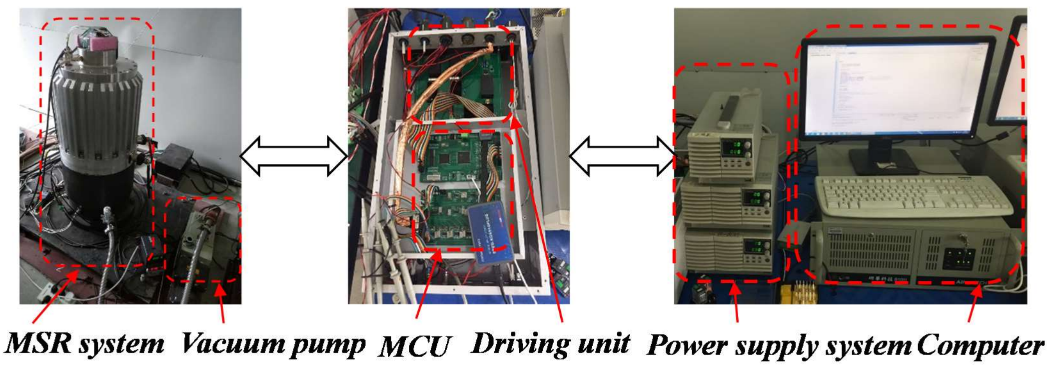

Fig. 5. Experimental setup.

Table 1. Parameters of the MSR System.

Parameter	***Value***	***Unit***
Equatorial moment of inertia	$J_x = 6.695$	kg m^2
Polar moment of inertia	$J_z = 1.477$	kg m^2
Radial current stiffness	$k_{iz} = 620$	N/A
Radial displacement stiffness	$k_{dz} = -2800$	N/mm
Axial current stiffness	$k_{iz} = 500$	N/A
Axial displacement stiffness	$k_{dz} = -1700$	N/mm
Displacement sensitivity	$k_s = 30$	V/mm
Rotor mass	$m = 150$	kg

The whole experimental setup in Fig. 5 contains three parts including the MSR system, microcontroller unit (MCU) and host computer. The rotor suspended by magnetic suspension system has five degrees of freedom. The vacuum pump is used to provide vacuum environment for MSR in order to reduce the friction loss. The MCU with 20kHz sampling frequency generates the control signal, and collect relative signal of MSR system such as control current, displacement of rotor, rotational speed and temperature. The MCU is composed of a digital signal processor chip (DSP TMS320F28335) and a FPGA chip with a 12-bit A/D convertor. The power supply system outputs 28V DC voltage to the whole control system, and the DC power supply provides the stable current for the magnetic suspension system. The driving unit based on a PWM amplifier with 20kHz drives winding. The host computer receive feedback signal including rotational speed and rotor displacement, and then send control command to the MCU for real-time monitoring of whole experimental setup system. Other system parameters are listed in Table 1.

4.3. Suspension Characteristics of MSR

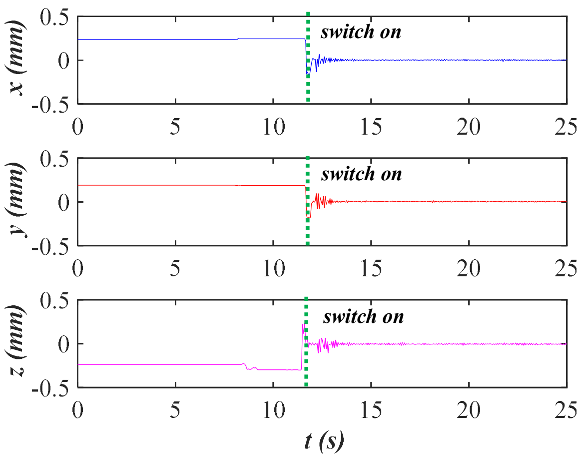

Fig. 6. Suspension in three directions.

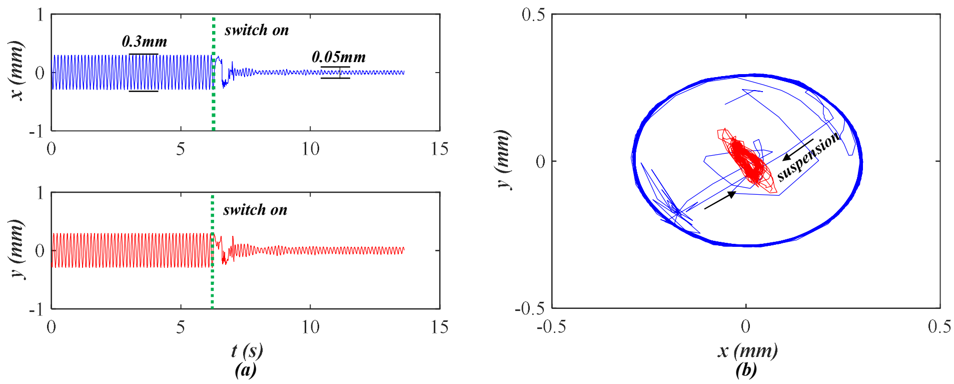

Fig. 7. Radial suspension, (a) radial displacement, (b) axis orbit.

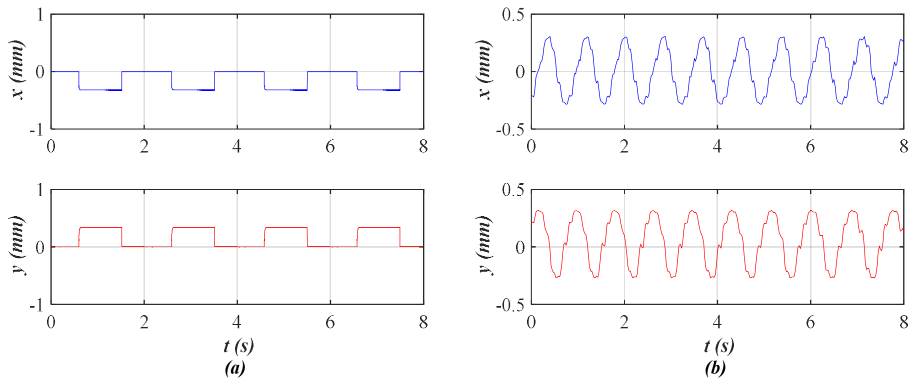

Fig. 8. Tilting suspension, (a) square tilting, (b) sine tilting.

The suspension process of MSR in axial and radial directions is shown in Fig. 6. When the magnetic suspension system is switched on, rotor displacements along three axes are equal to zero. It means the MSR is stably suspended at the equilibrium point in radial and axial directions. In addition, the radial suspension procedure of MSR can be indicated by the axis orbit as illustrated in Fig. 7. When the MSR is not forced to suspend at the equilibrium point in radial direction, the axis orbit of MSR is the blue cycle with radius 0.3mm. The red cycle represents the axis orbit with radius 0.05mm when the MSR is suspended at the equilibrium point in radial direction. Therefore, the axis orbit of the MSR can verify that the rotor is stably suspended at the equilibrium point in radial direction.

Moreover, the active controllability of MSR is verified by regulating the control current of the winding. As illustrated in Fig. 8, control currents with sine current and square current are applied to control the tilting of the MSR around radial axes (x axis and y axis). Fig. 8(a) is the square tilting of MSR, the duty ratio is 50%, and the amplitude is 0.3mm. Fig. 8(b) is the sine tilting of MSR, the amplitude is 0.3mm, and the tilting frequency is 1Hz. Therefore, the AMB can suppress the vibration and disturbance of the MSR by regulating system parameters based on the displacement feedback.

4.4. Rotation Characteristics of MSR

In order to test the rotation characteristics of the MSR, the rotor displacements and vibration magnitudes of MSR at different rotational frequencies are measured. The vibration response of MSR with 20Hz is shown in Fig. 9. As shown in Fig. 9(a), the maximum deflection displacement of MSR is about 0.04mm. The axis orbit of MSR is illustrated in Fig. 9(b), and the vibration magnitude of resonance is -33dB as shown in Fig. 9(c). When the rotational frequency increases to 60Hz, the vibration of MSR is shown in Fig. 10. The maximum deflection displacement is 0.04mm in Fig. 10(a). The axis orbit of the rotor is shown in Fig. 10(b), and vibration magnitude is about -27dB in Fig. 10(c). When the rotational frequency is 100Hz, the vibration of MSR is shown in Fig. 11. The axis orbit of the rotor is illustrated in Fig. 11(b). The deflection displacement is about 0.034mm, and the vibration magnitude is -30dB. The vibration magnitudes from 20Hz to 100Hz are shown in Fig. 12(a). It shows that the vibration magnitude of resonance decreases with rotational frequency. Moreover, the nutation frequency of MSR is proportional to the rotational frequency in Fig. 12(b). Therefore, when the MSR runs at high frequency, the nutation seriously affects the stability. Consequently, the results indicate that the rotation characteristics of the MSR including the resonant vibration, precession vibration and nutation vibration can be regulated by the control parameters based on the feedback system.

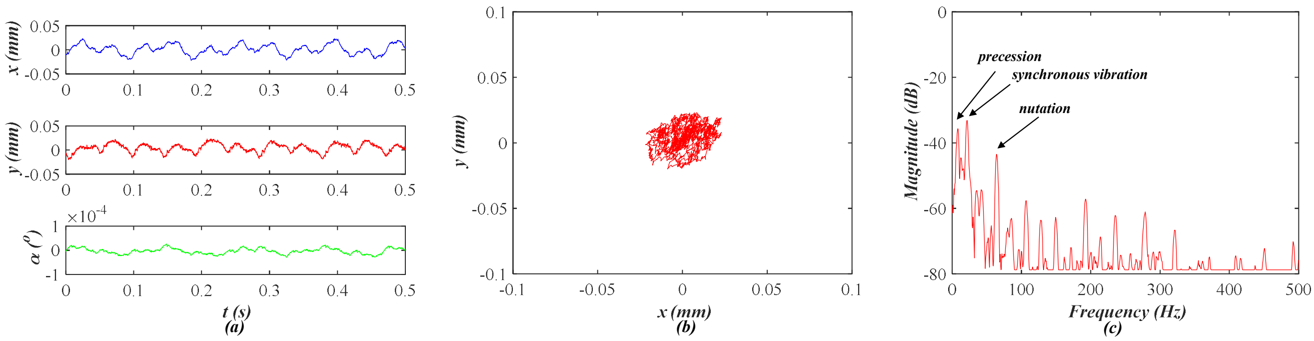

Fig. 9. Vibration with 20Hz, (a) rotor displacement, (b) axis orbit, (c) vibration magnitude.

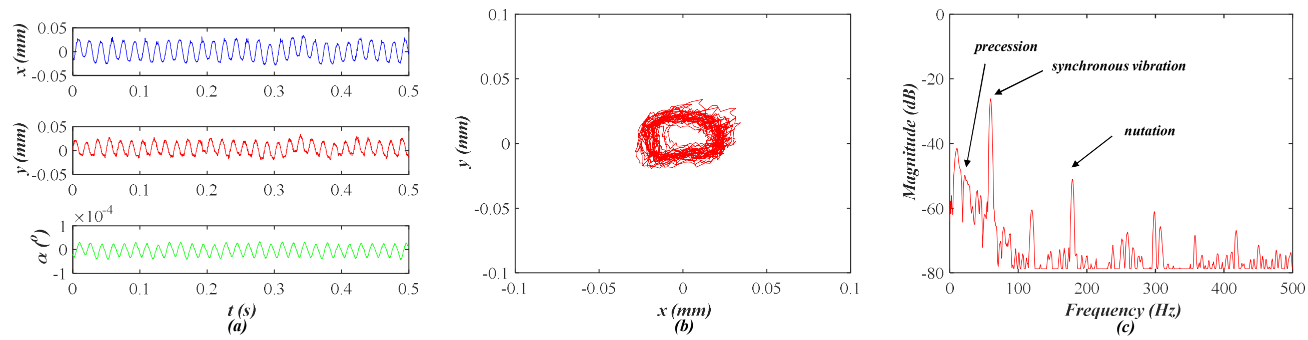

Fig. 10. Vibration with 60Hz, (a) rotor displacement, (b) axis orbit, (c) vibration magnitude.

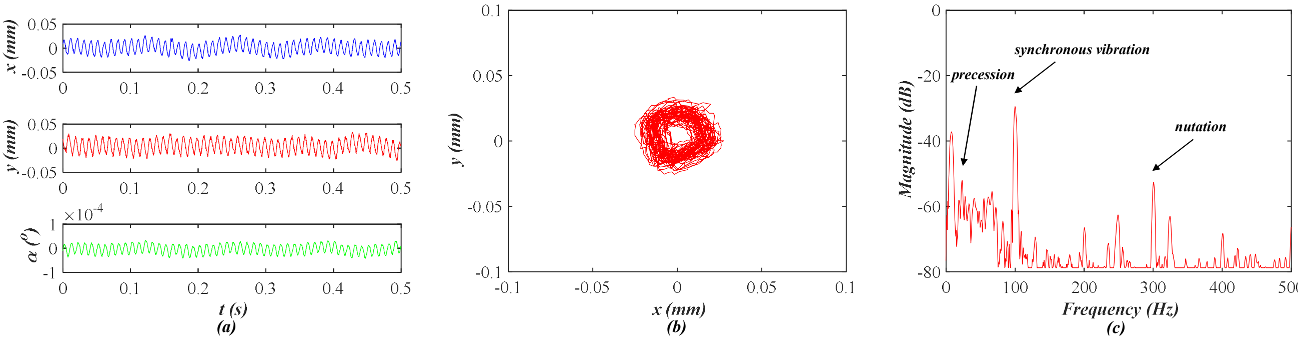

Fig. 11. Vibration with 100Hz, (a) rotor displacement, (b) axis orbit, (c) vibration magnitude.

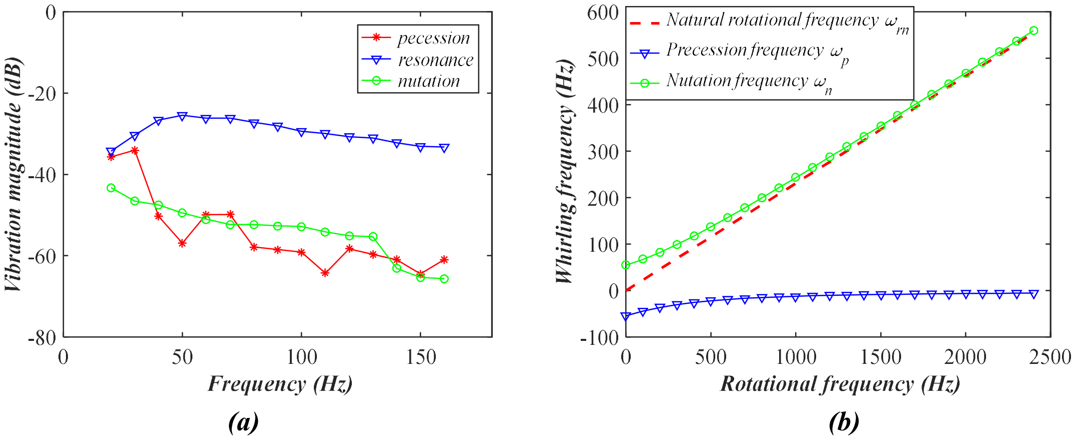

Fig. 12. Relationship between rotation characteristics and rotational frequency, (a) magnitude, (b) frequency.

4.5. Vibration Transmissibility of MSR

The relationship between the vibration characteristics of the MSR and the proportional coefficient k_P is illustrated in Fig. 13(a). When $k_P = 10$, the natural frequency of MSR is about 3Hz, and the natural frequency increases to 20Hz when $k_P = 150$ as shown in Fig. 13(b). It indicates that the natural frequency of MSR increases with the proportional coefficient. The relationship between the vibration transmissibility and the proportional coefficient is shown as Fig. 13(c), it shows that the vibration transmissibility of MSR increases with the proportional coefficient. Consequently, the results present that the natural frequency and transmissibility of the MSR can be regulated by proportional coefficient.

Moreover, the relationship between the vibration characteristics of MSR and the derivative coefficient k_D is shown in Fig. 14(a). When $k_D = 0.005$, the transmissibility amplitude is about 22, and it decreases to 1.2 when $k_D = 5$. The vibration transmissibility decreases with derivative coefficient as shown in Fig. 14(c). Moreover, the relationship between the natural frequency ω_n and derivative coefficient k_D is shown in Fig. 14(b). The natural frequency of the MSR is constant 10.75Hz while the derivative coefficient varies. Therefore, the transmissibility amplitude of the MSR can be mitigated by regulating the derivative coefficient, while the natural frequency of the MSR is not affected.

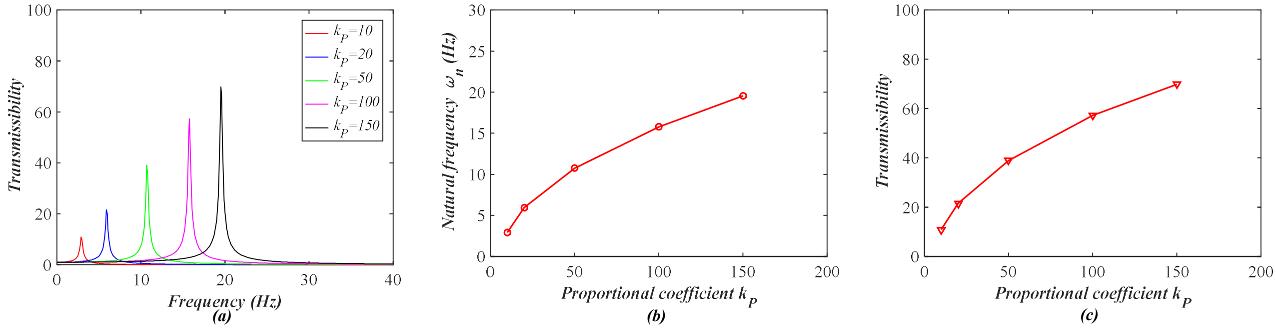

Fig. 13. Relationship between vibration characteristics and proportional coefficient, (a) response, (b) natural frequency, (c) transmissibility magnitude.

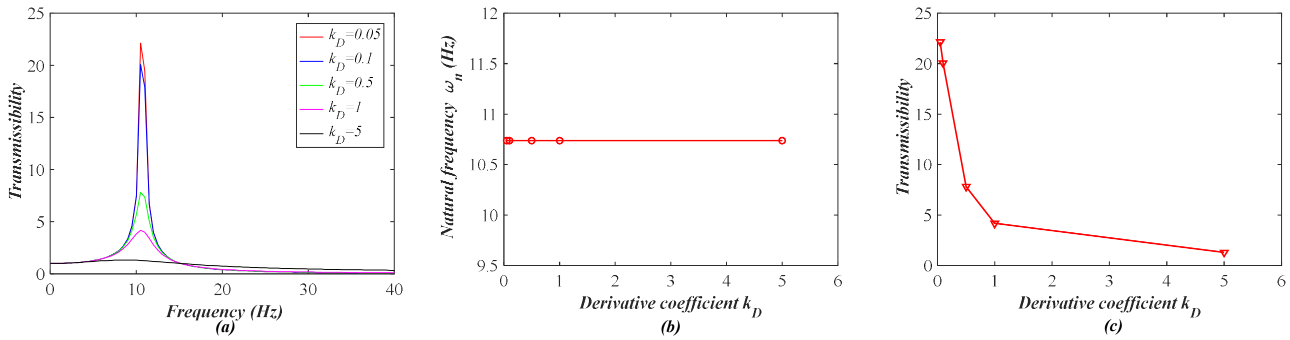

Fig. 14. Relationship between vibration characteristics and derivative coefficient, (a) response, (b) natural frequency, (c) transmissibility magnitude.

4.6. Tilting Angle Response of MSR with Disturbance Input

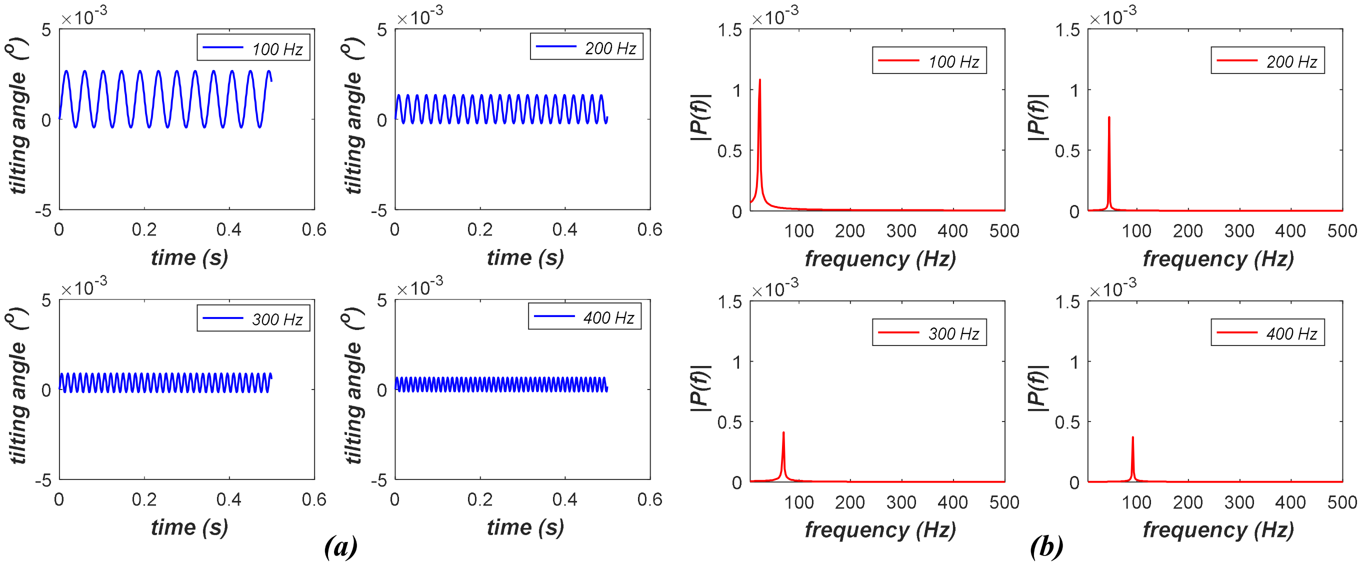

Fig. 15. Tilting angle response with impulse torque disturbance, (a) angle amplitude, (b) amplitude spectrum.

The tilting angle response of MSR with impulse torque disturbance is shown in Fig. 15(a), and amplitude spectra is shown in Fig. 15(b). The tilting angle varies with the rotational frequency. The frequency of titling angle is the natural rotational frequency, and the amplitude of tilting angle decreases with rotational frequency.

As shown in Fig. 16, the tilting angle response of MSR decreases with the rotational frequency. In addition, according to the amplitude spectrum in Fig. 16(b), the tilting angle response of MSR has obvious vibration when the frequency equals to the natural rotational frequency.

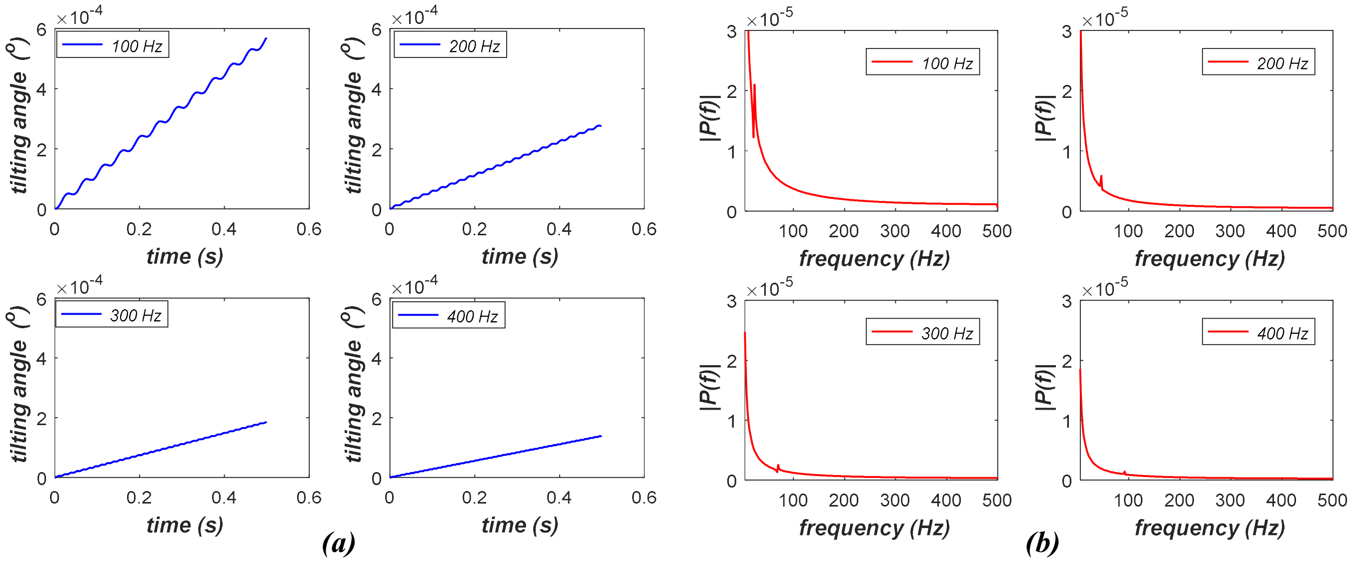

Fig. 16. Tilting angle response of constant torque disturbance, (a) angle amplitude, (b) amplitude spectrum.

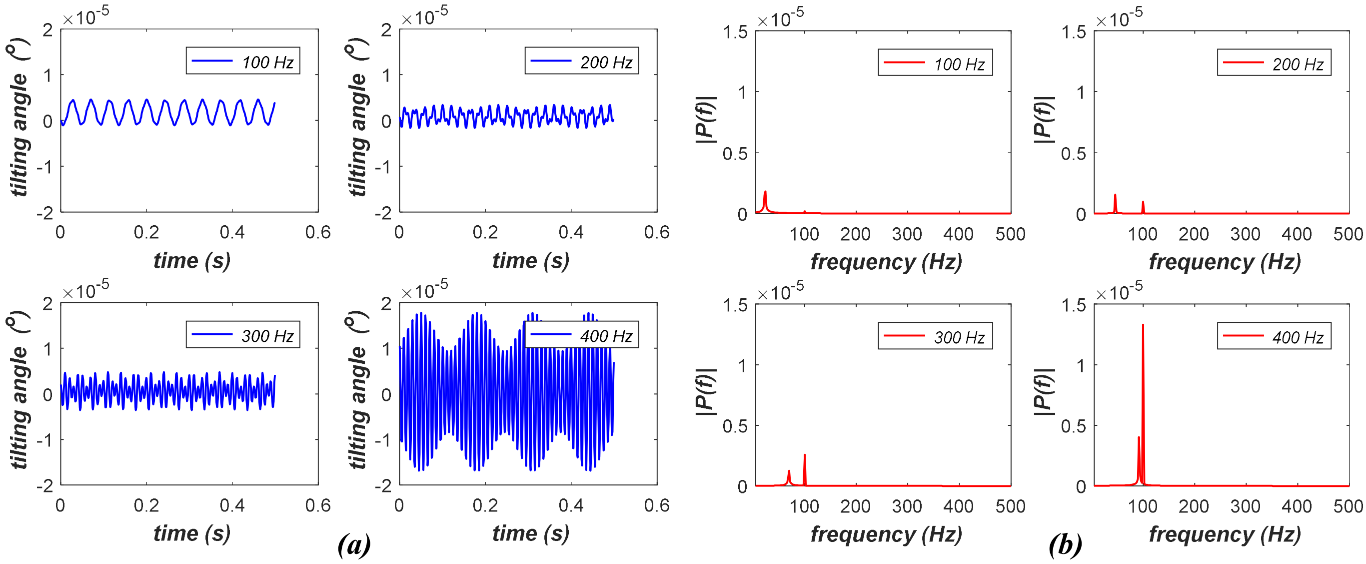

Fig. 17. Tilting angle response of harmonic torque disturbance, (a) angle amplitude, (b) amplitude spectrum.

As illustrated in Fig. 17, the tilting angle response of MSR with the harmonic torque disturbance contains rotation vibration with two different frequencies (the natural rotational frequency of rotor and the frequency of harmonic torque), and its amplitude increases with rotational frequency. Based on the amplitude spectrum in Fig. 17(b), the tilting angle response has obvious variations at the respective natural rotational frequency and frequency of harmonic disturbance.

5. Conclusion

The vibration characteristics of a MSR with AMBs in a flywheel energy storage system are investigated. The vibration transmissibility of the MSR decreases with the derivative coefficient of the control system. The natural frequency is positively linear to the proportional coefficient, and the transmissibility increases with the proportional coefficient of the control system. This results provide the method for the vibration suppression of the MSR. Furthermore, the rotor displacements and vibration amplitudes of MSR at different rotational frequencies are measured to investigate the rotational dynamics in experiments. Results indicate that the rotor displacement decreases with the rotational frequency based on the feedback system. Moreover, the tilting angle response of the MSR is affected by the frequency of the disturbance inputs. Therefore, the detailed relationship between vibration characteristics and system parameters of MSR will be useful in the design and control of the MSR in flywheel energy storage system.

References

[1] M. Ahrens, L. Kucera, R. Larsonneur, Performance of a magnetically suspended flywheel energy storage device, IEEE Transactions on control systems technology, 4 (1996) 494-502.

[2] B. Xiang, J. Tang, Suspension and titling of vernier-gimballing magnetically suspended flywheel with conical magnetic bearing and Lorentz magnetic bearing, Mechatronics, 28 (2015) 46-54.

[3] J. Fang, Y. Ren, High-precision control for a single-gimbal magnetically suspended control moment gyro based on inverse system method, IEEE Transactions on Industrial Electronics, 58 (2011) 4331-4342.

[4] Y. Ren, J. Fang, High-stability and fast-response twisting motion control for the magnetically suspended rotor system in a control moment gyro, IEEE/ASME Transactions on Mechatronics, 18 (2013) 1625-1634.

[5] Y. Ren, D. Su, J. Fang, Whirling modes stability criterion for a magnetically suspended flywheel rotor with significant gyroscopic effects and bending modes, IEEE Transactions on Power Electronics, 28 (2013) 5890-5901.

[6] J. Fang, S. Zheng, B. Han, AMB vibration control for structural resonance of double-gimbal control moment gyro with high-speed magnetically suspended rotor, IEEE/ASME Transactions on Mechatronics, 18 (2013) 32-43.

[7] T. Schneeberger, T. Nussbaumer, J.W. Kolar, Magnetically levitated homopolar hollow-shaft motor,

IEEE/ASME transactions on mechatronics, 15 (2010) 97-107.
[8] X. Sun, L. Chen, Z. Yang, Overview of bearingless permanent-magnet synchronous motors, IEEE Transactions on Industrial Electronics, 60 (2013) 5528-5538.
[9] S. Zheng, R. Feng, Feedforward compensation control of rotor imbalance for high-speed magnetically suspended centrifugal compressors using a novel adaptive notch filter, Journal of Sound and Vibration, 366 (2016) 1-14.
[10] J. Asama, D. Kanehara, T. Oiwa, A. Chiba, Development of a compact centrifugal pump with a two-axis actively positioned consequent-pole bearingless motor, IEEE Transactions on Industry Applications, 50 (2014) 288-295.
[11] S. Cheng, M.W. Olles, D.B. Olsen, L.D. Joyce, S.W. Day, Miniaturization of a magnetically levitated axial flow blood pump, Artificial organs, 34 (2010) 807-815.
[12] B. Han, Q. Xu, Q. Yuan, Multiobjective optimization of a combined radial-axial magnetic bearing for magnetically suspended compressor, IEEE Transactions on Industrial Electronics, 63 (2016) 2284-2293.
[13] T. Masuzawa, S. Ezoe, T. Kato, Y. Okada, Magnetically suspended centrifugal blood pump with an axially levitated motor, Artificial organs, 27 (2003) 631-638.
[14] T. Masuzawa, T. Kita, K.i. Matsuda, Y. Okada, Magnetically Suspended Rotary Blood Pump with Radial Type Combined Motor‐Bearing, Artificial organs, 24 (2000) 468-474.
[15] J. Sun, C. Wang, Y. Le, Designing and Experimental Verification of the Axial Hybrid Magnetic Bearing to Stabilization of a Magnetically Suspended Inertially Stabilized Platform, IEEE/ASME Transactions on Mechatronics, 21 (2016) 2881-2891.
[16] Q. Guo, G. Liu, B. Xiang, H. Liu, T. Wen, The disturbance rejection of magnetically suspended inertially stabilized platform, Transactions of the Institute of Measurement and Control, (2016) 0142331216661623.
[17] Q. Guo, G. Liu, B. Xiang, T. Wen, H. Liu, Robust control of magnetically suspended gimbals in inertial stabilized platform with wide load range, Mechatronics, 39 (2016) 127-135.
[18] X. Ren, Y. Le, B. Han, K. Wang, Loss optimization and thermal analysis of a heteropolar magnetic bearing for a vacuum turbo-molecular pump, International Journal of Applied Electromagnetics and Mechanics, 54 (2017) 673-690.
[19] X. Ren, Y. Le, B. Han, System Electromagnetic Loss Analysis and Temperature Field Estimate of

a Magnetically Suspended Motor, Progress In Electromagnetics Research M, 55 (2017) 51-61.
[20] Z. Huang, J. Fang, X. Liu, B. Han, Loss calculation and thermal analysis of rotors supported by active magnetic bearings for high-speed permanent-magnet electrical machines, IEEE Transactions on Industrial Electronics, 63 (2016) 2027-2035.
[21] K. Jiang, C. Zhu, Multi-frequency periodic vibration suppressing in active magnetic bearing-rotor systems via response matching in frequency domain, Mechanical Systems and Signal Processing, 25 (2011) 1417-1429.
[22] M. Cole, P. Keogh, C. Burrows, Vibration control of a flexible rotor/magnetic bearing system subject to direct forcing and base motion disturbances, Proceedings of the Institution of Mechanical Engineers, Part C: Journal of Mechanical Engineering Science, 212 (1998) 535-546.
[23] Q. Chen, G. Liu, S. Zheng, Suppression of imbalance vibration for AMBs controlled driveline system using double-loop structure, Journal of Sound and Vibration, 337 (2015) 1-13.
[24] X. Xu, S. Chen, Y. Zhang, Automatic balancing of AMB systems using plural notch filter and adaptive synchronous compensation, Journal of Sound and Vibration, 374 (2016) 29-42.
[25] J. Asama, M. Amada, N. Tanabe, N. Miyamoto, A. Chiba, S. Iwasaki, M. Takemoto, T. Fukao, M.A. Rahman, Evaluation of a bearingless PM motor with wide magnetic gaps, IEEE Transactions on Energy Conversion, 25 (2010) 957-964.
[26] J. Tang, B. Xiang, Y. Zhang, Dynamic characteristics of the rotor in a magnetically suspended control moment gyroscope with active magnetic bearing and passive magnetic bearing, ISA transactions, 53 (2014) 1357-1365.
[27] J. Ji, C. Hansen, Non-linear oscillations of a rotor in active magnetic bearings, Journal of Sound and vibration, 240 (2001) 599-612.
[28] J. Ji, L. Yu, A. Leung, Bifurcation behavior of a rotor supported by active magnetic bearings, Journal of Sound and Vibration, 235 (2000) 133-151.
[29] Y. Yan, D. Zhiquan, Z. Qianying, W. Xiaolin, Stator vibration analysis of bearingless switched reluctance motors, in: Electrical and Control Engineering (ICECE), 2010 International Conference on, IEEE, 2010, pp. 1993-1996.
[30] S.-M. Yang, Electromagnetic actuator implementation and control for resonance vibration reduction in miniature magnetically levitated rotating machines, IEEE Transactions on Industrial Electronics, 58 (2011) 611-617.

[31] J. Tang, K. Wang, Z. Peng, S. Zhao, Mechanical characteristics analysis of high-speed rotor in magnetically suspended control moment gyroscope, Transactions of the Institute of Measurement and Control, (2016) 0142331216678448.